membranes

MDPI

*Review*

# Voltage Dependence of $Na^+/K^+$-ATPase: From Electrogenic Transport to Isoform-Specific Physiology

**Pauline R. V. Mansur [1], Antônio-Carlos G. de Almeida [1], Arthur C. Pires [1], Carla A. Scorza [2], Fulvio A. Scorza [2] and Antônio M. Rodrigues [1,*]**

[1] Bioengineering Program, Department of Biotechnology, Federal University of São João del-Rei, São João del-Rei 36301-160, Brazil; paulinemansur@gmail.com (P.R.V.M.); acga@ufsj.edu.br (A.-C.G.d.A.); arthurcpires@hotmail.com (A.C.P.)

[2] Department of Experimental Neurology, Paulista School of Medicine, Federal University of São Paulo, São Paulo 04023-062, Brazil; carla.scorza@unifesp.br (C.A.S.); scorza@unifesp.br (F.A.S.)

* Correspondence: amr@ufsj.edu.br

## Abstract

Membrane potential influences $Na^+/K^+$-ATPase function through coupled energetic and kinetic mechanisms that shape its electrogenic current across the cell membrane. This conceptual integrative review integrates electrophysiological, structural, isoform-specific, and modeling evidence to distinguish three levels of description: net charge transported per canonical cycle, voltage-dependent cycle free energy, and voltage-sensitive microscopic transition rates. Classic experiments identify extracellular $Na^+$ release and rebinding as major sources of voltage sensitivity, while $K^+$-associated transients reveal additional field-sensitive binding steps. Recent structural intermediates constrain candidate reaction pathways, but their correspondence to electrical distances and relaxation components requires functional testing. Isoform comparisons demonstrate that voltage-dependent recruitment depends on subunit composition and experimental conditions. A comparison of published models and an illustrative two-state calculation shows that thermodynamic consistency constrains rate ratios but does not uniquely determine relaxation kinetics. Overall, membrane-voltage dependence emerges from the interaction between cycle thermodynamics, ion translocation, and voltage-sensitive microscopic transitions. Predictive descriptions should therefore preserve cycle energetics, report ionic and metabolic conditions, and retain the states needed for their intended observables. Joint analysis of current–voltage relations, charge movement, and relaxation kinetics offers a practical route to testing competing mechanisms without assuming unique parameter identification.

**Keywords:** $Na^+/K^+$-ATPase; membrane potential; electrogenicity; voltage dependence; Albers–Post cycle; pump current; thermodynamics; kinetic modeling

Check for updates

Academic Editors: Hsueh-Chia Chang and Jean Chemin

Received: 2 November 2026
Revised: 24 November 2026
Accepted: 26 November 2026
Published: 28 November 2026

**Copyright:** © 2026 by the authors. Licensee MDPI, Basel, Switzerland. This article is an open access article distributed under the terms and conditions of the Creative Commons Attribution (CC BY) license.

## 1. Introduction

The $Na^+/K^+$-ATPase couples ATP hydrolysis to the active extrusion of $Na^+$ and uptake of $K^+$, thereby maintaining transmembrane ionic gradients essential for cellular excitability and secondary active transport [1,2]. Within the canonical Albers–Post conformational framework, the enzyme exports three intracellular $Na^+$ ions and imports two extracellular $K^+$ ions per ATP molecule hydrolyzed [2–4]. This 3:2 transport stoichiometry results in the net outward movement of one positive charge per completed cycle, establishing the electrogenic nature of the $Na^+/K^+$-ATPase and its direct contribution to membrane electrophysiology [2,5]. The physiological relevance of this electrogenicity becomes particularly

evident under conditions of pronounced ionic imbalance, such as nonsynaptic epileptiform activity induced by elevated extracellular $K^+$ and reduced extracellular $Ca^{2+}$ concentrations. Under these conditions, intracellular $Na^+$ accumulation can stimulate electrogenic pump activity, contributing to neuronal repolarization and potentially playing a critical role in terminating sustained paroxysmal discharges [6]. Beyond its contribution to membrane polarization, however, the electrogenic nature of the $Na^+/K^+$-ATPase also establishes a fundamental relationship between membrane voltage, the energetics of ion transport, and the kinetics of the underlying catalytic reactions.

This review distinguishes three conceptually distinct but physically coupled quantities (Figure 1): the net charge transported per canonical cycle, the voltage-dependent free-energy balance of that cycle, and the voltage dependence of individual microscopic transition rates. Net electrogenicity describes the charge balance of completed canonical 3:2 cycles without specifying how charge displacement is distributed among intermediate transitions [7,8]. Thermodynamic voltage dependence describes how membrane potential contributes to the free-energy balance of the coupled cycle and defines its thermodynamic reversal condition without, by itself, determining the rate at which the cycle proceeds [9,10]. Microscopic kinetic voltage dependence describes how the forward and reverse rates of individual partial reactions vary with membrane potential as ions and charge-bearing conformational rearrangements move through fractions of the transmembrane electric field [11–13]. The extracellular access-channel concept provides a mechanistic framework for interpreting field-sensitive ion binding and release [14,15]. Under the experimental conditions studied, extracellular $Na^+$ release and rebinding constitute a major established source of voltage dependence of the pump, whereas $K^+$-associated reactions contribute through kinetically distinct steps [16,17]. These levels are physically coupled and thermodynamically constrained, yet distinct. Their separation provides a framework for integrating classic voltage-clamp and charge-movement measurements with structural intermediates observed under turnover conditions and with thermodynamically consistent kinetic models [10,18,19].

Voltage-clamp studies established that $Na^+/K^+$ pump current depends nonlinearly on membrane potential and that extracellular $Na^+$ strongly shapes this relationship [5,7,11]. Subsequent pre-steady-state measurements linked a major component of this voltage dependence to extracellular $Na^+$ binding, deocclusion, and release through a field-sensitive access pathway, resolving kinetically distinct components associated with the sequential release of the three $Na^+$ ions [12–15,20].

Concurrently, the molecular interpretation of these electrophysiological phenomena has become substantially richer. High-resolution structural studies have resolved ion-binding configurations associated with $Na^+$- and $K^+$-bound states and large conformational differences in the catalytic α-subunit within the E1/E2 transport cycle. In particular, the 2.4 Å structure of the $Na^+/K^+$-ATPase in an E2·2$K^+$·$P_i$-like state visualized the transmembrane $K^+$-binding sites, associated water molecules, the phosphorylation-site phosphate analogue, and the contribution of the β-subunit to $K^+$ coordination [21–23]. More recently, cryo-EM structures obtained under ATP-activated turnover conditions captured multiple $Na^+$-bound intermediates, including $Na_2$E1-ATP, [$Na_3$]E1P-ADP, and [$Na_3$]E2P, providing structural constraints for interpreting the sequence of $Na^+$ binding, occlusion, and extracellular release [19]. In parallel, biochemical and spectroscopic studies indicate that the E1/E2 conformational equilibrium and transition kinetics are sensitive to ionic strength, divalent cations, and the electrostatic environment at the membrane–protein interface [24–26]. Taken together, these findings suggest that macroscopic voltage dependence should not be represented by a single phenomenological factor without specifying the microscopic transition and charge displacement to which that dependence is assigned. Structural intermediates

constrain the states through which the enzyme progresses, but do not, by themselves, determine the electrical distance or voltage dependence of individual transitions [19,22].

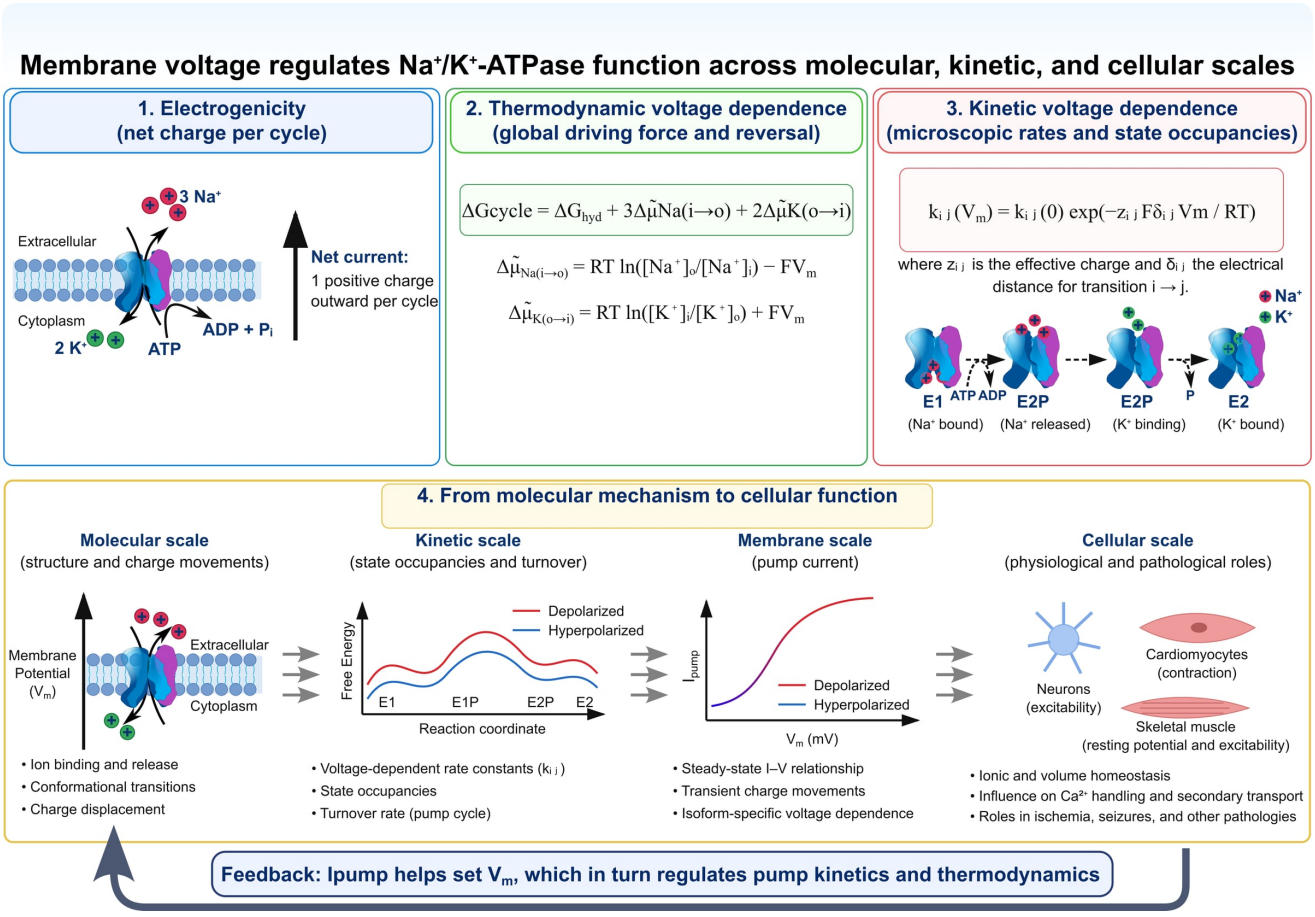


**Figure 1.** Multiscale framework for membrane-voltage regulation of $Na^+/K^+$-ATPase. Electrogenicity, cycle thermodynamics, and microscopic transition kinetics are distinct but coupled descriptions. All curves and energy profiles are qualitative schematics, without fitted parameters or measured state probabilities. The kinetic energy profile depicts candidate barriers along a reaction coordinate; state occupancies are a separate consequence of the transition network. The voltage convention is $V_m = \psi_i - \psi_o$.

Despite these advances, a unified interpretation of voltage regulation remains challenging because electrophysiological, structural, and modeling approaches provide constraints on different aspects of pump function. Voltage-clamp and pre-steady-state measurements directly constrain voltage-dependent pump currents and specific field-sensitive partial reactions [8,18]. Mechanistic models provide the framework needed to connect these observations, but local assignments of voltage sensitivity must remain compatible with both experimental observables and the thermodynamic constraints of the complete transport cycle [10,27,28]. Consequently, macroscopic voltage dependence generally cannot be uniquely assigned to a microscopic mechanism from steady-state measurements alone; discrimination among competing mechanisms requires integration of these complementary constraints.

Previous reviews have generally emphasized particular aspects of $Na^+/K^+$-ATPase function, including electrogenic transport, transient currents, and cardiac electrophysiology [29–31]. These contributions established important experimental and mechanistic foundations, but the relationship among net electrogenicity, cycle-level thermodynamics, and voltage-dependent microscopic kinetics has rarely been examined as a single analytical problem. In particular, the extent to which macroscopic current–voltage behavior constrains

the allocation of electrical displacement and the rate constants of individual transitions remains unresolved. Here, we address this gap by integrating these complementary lines of evidence and by examining their implications for structural intermediates, isoform-specific physiology, and thermodynamically constrained kinetic models.

This conceptual integrative review examines how transport stoichiometry, cycle thermodynamics, transient electrical measurements, structural intermediates, and isoform-specific physiology constrain the membrane-voltage dependence of the $Na^+/K^+$-ATPase. The literature was analyzed across four complementary domains: electrophysiological measurements of steady-state and transient pump currents, structural studies of ion-bound and conformational intermediates, isoform- and subunit-specific functional studies, and thermodynamically constrained kinetic models. Studies were considered according to their mechanistic relevance to at least one of three analytical levels: net charge transported per cycle, voltage-dependent free-energy balance, and voltage-sensitive microscopic transition rates. The following sections apply this framework to the electrophysiological, structural, isoform-specific, and kinetic-modeling evidence reviewed in the literature.

The purpose of this integration was to compare the constraints provided by different experimental and theoretical approaches. Particular attention was given to experimental conditions, ionic and metabolic composition, preparation type, temporal resolution, model assumptions, and the distinction between directly measured observables and mechanistic interpretations. When studies appeared to provide conflicting conclusions, the differences were interpreted in relation to their experimental protocols, isoform or subunit composition, state occupancy, and kinetic-model structure. The resulting framework therefore distinguishes established observations, model-dependent assignments, and hypotheses requiring further functional testing. Figures 1–3, prepared using Inkscape (version 1.3; Inkscape Project, https://inkscape.org/), illustrate the framework and its physiological implications.

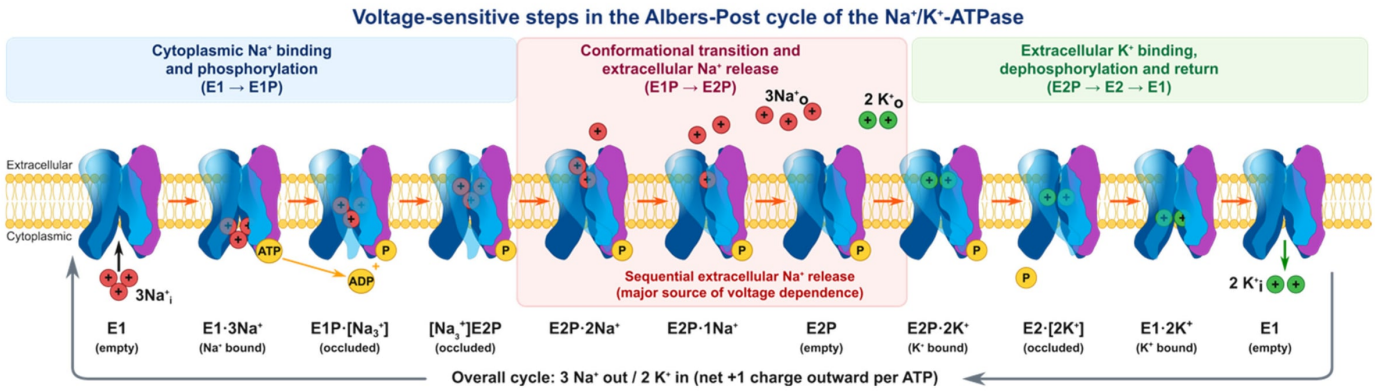


**Figure 2.** Candidate voltage-sensitive reactions in the Albers–Post cycle.

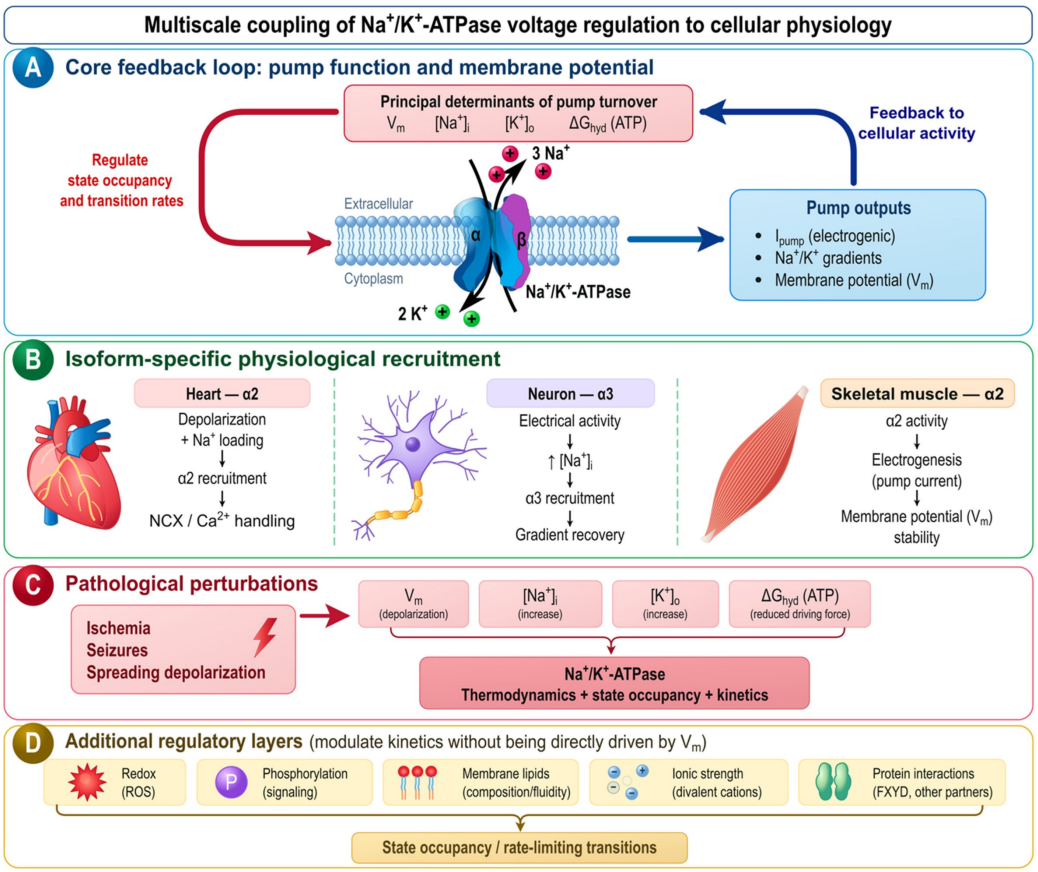


**Figure 3.** Coupling of pump regulation to cellular physiology. (**A**) Feedback among turnover, membrane potential, and ionic gradients. (**B**) Isoform-dependent recruitment and physiological context. (**C**) Pathological changes in voltage, ions, and ATP-hydrolysis free energy jointly affect pump behavior; their direction and magnitude depend on condition, phase, and severity. Reduced metabolic driving force is not assumed for every seizure. (**D**) Additional mechanisms affect occupancy and rates. All panels are qualitative schematics, not quantitative predictions.

## 2. $Na^+/K^+$-ATPase as an Electrogenic Transporter

In the canonical forward cycle, the $Na^+/K^+$-ATPase exports three cytoplasmic $Na^+$ ions and imports two extracellular $K^+$ ions per ATP molecule hydrolyzed [2,4,7]:

$$3Na_i^+ + 2K_o^+ + ATP \rightleftharpoons 3Na_o^+ + 2K_i^+ + ADP + P_i. \quad (1)$$

The completed canonical cycle produces a net outward displacement equivalent to one positive elementary charge. For a molar cycle flux density $J_{cycle}$, expressed in $mol.m^{-2}.s^{-1}$, the current density generated by tightly coupled canonical transport is therefore

$$I_{pump} = FJ_{cycle}, \quad (2)$$

where $F$ is Faraday's constant and outward current is defined as positive. This stoichiometric relation specifies the net charge balance, not its allocation among elementary reactions [29]. Its distribution among elementary reactions is further constrained by transient-current experiments and the kinetic formalism described in Section 4 .

Under controlled conditions, cardiotonic steroid-sensitive holding currents provide an operational measure of the pump-generated outward current [30]. A change in resting potential is less specific because its magnitude also depends on background conductances and changing ion gradients. Thus, demonstrating that pump activity changes membrane potential does not establish how an imposed voltage changes microscopic pump rates. Direct

tests require voltage control and measurement of pump current or charge displacement under specified ionic and nucleotide conditions [11,12]. Section 8 considers physiological examples of feedback from membrane voltage and ionic gradients to pump activity. This physiological relevance is particularly evident in the nervous system, where impaired $Na^+/K^+$-ATPase function may compromise ionic homeostasis and contribute to excitotoxic and inflammatory processes associated with neurological disease [32].

## 3. Thermodynamic Basis of Voltage Dependence

Thermodynamic voltage dependence concerns the free-energy balance of the complete coupled reaction, rather than the rate of a particular molecular step. Because the $Na^+/K^+$-ATPase exports three $Na^+$ ions and imports two $K^+$ ions per cycle, the electrical contributions do not cancel, and membrane voltage contributes directly to the free-energy balance of forward transport [9,30].

$$\Delta\tilde{\mu}_X = RT\, ln\frac{a_{X,2}}{a_{X,1}} + z_X F(\psi_2 - \psi_1), \tag{3}$$

where $a_X$ is the activity of ion X, $z_X$ its valence, $F$ Faraday's constant, $R$ the gas constant, and $T$ the absolute temperature.

Throughout this review, $V_m = \psi_i - \psi_o$, and the forward cycle hydrolyzes one ATP molecule. $\Delta G_{hyd}$ denotes the actual molar Gibbs free-energy change in ATP hydrolysis, evaluated under a consistent convention for nucleotide, phosphate, pH, $Mg^{2+}$, and temperature. With these definitions, the electrical contribution to the forward cycle is $-FV_m$ because three $Na^+$ ions move outward and two $K^+$ ions move inward. A more negative $Vm$ therefore increases the electrical cost of forward transport [28].

$$\Delta G_{cycle} = \Delta G_{hyd} + 3RT\, ln\frac{a_{Na,o}}{a_{Na,i}} + 2RT\, ln\frac{a_{K,i}}{a_{K,o}} - FV_m. \tag{4}$$

For a tightly coupled 3:2:1 transport cycle, the thermodynamic reversal condition is $\Delta G_{cycle} = 0$. At this condition, the net flux of the coupled cycle and the corresponding canonical steady-state pump current vanish. At fixed ion and metabolite activities, the associated reversal potential is given by Equation (5). Negative values of $\Delta G_{cycle}$ favor forward transport, whereas positive values favor the reverse coupled reaction, which could include ATP synthesis if reverse transitions are kinetically accessible and ADP and inorganic phosphate (Pi) are available. This thermodynamic criterion determines neither the rate of reversal nor whether ATP depletion alone is sufficient to drive reverse operation [10,30].

$$V_{rev} = \frac{\Delta G_{hyd} + 3RT\, ln\frac{a_{Na,o}}{a_{Na,i}} + 2RT\, ln\frac{a_{K,i}}{a_{K,o}}}{F}. \tag{5}$$

This constraint is essential for kinetic modeling: a model may reproduce a physiological I–V (current–voltage relation) curve while violating the thermodynamic free-energy balance of the complete cycle. Thermodynamic consistency therefore requires detailed balance at equilibrium and local coupling of rates to chemical and electrical potentials away from equilibrium [10,27,28].

Thermodynamic consistency constrains the cycle affinity, reversal condition, and local ratios of forward and reverse rates, but does not uniquely determine absolute rate magnitudes, relaxation times, or the shape of the I–V relation away from equilibrium. These observables also depend on the distribution of electrical displacement, state occupancies, and rate-limiting transitions. Consequently, thermodynamically consistent schemes may share the same cycle affinity and reversal potential while predicting different steady-state and transient behavior [9,10,33].

Metabolic and ionic disturbances alter cycle affinity through distinct energetic terms. A less negative $\Delta G_{hyd}$ weakens the hydrolytic driving force, whereas increased intracellular $Na^+$, extracellular $K^+$, or depolarization reduces the opposing chemical or electrical work of forward transport. These changes also affect ligand binding and state occupancy; therefore, the overall ischemic response cannot be represented by a single empirical voltage factor [28,34]. Conversely, hypoxic conditioning can also enhance pump-dependent electrogenesis in a tissue- and isoform-specific manner: short-term hypobaric hypoxia increased the electrogenic activity of the α2 isoform and produced sustained sarcolemmal hyperpolarization in rat diaphragm, without increasing total α2-subunit abundance [35]. Metabolic consequences also depend on the rate and pathway of pump turnover, rather than solely on the free energy dissipated per completed cycle. Kinetic simulations indicate that $Na^+/K^+$-ATPase-associated heat production depends on pump activity, passive ion permeability, and the relative contribution of alternative transport pathways, linking cycle thermodynamics to whole-cell energetic demand [36].

## 4. Molecular and Kinetic Basis of Voltage Dependence in the Albers–Post Cycle

The Albers–Post scheme identifies reaction steps that could be voltage-sensitive: $Na^+$ binding to E1, phosphorylation-coupled $Na^+$ occlusion, the E1P-to-E2P transition, extracellular $Na^+$ release, $K^+$ binding, dephosphorylation-coupled $K^+$ occlusion, and the E2-to-E1 transition associated with cytoplasmic $K^+$ release [2,22] (Figure 2). Voltage can influence steps that displace ionic or protein charge through the membrane field, including access to buried binding sites [12,14].

Three observations implicate extracellular $Na^+$ release and rebinding as a major source of voltage dependence: removing extracellular $Na^+$ greatly reduces steady-state voltage dependence; electroneutral $Na^+/Na^+$ exchange remains voltage sensitive; and voltage jumps evoke transient charge movements when turnover is restricted to the $Na^+$ branch [11,12,37]. These findings are consistent with a high-field extracellular access pathway proposed in microscopic models and supported by functional studies [12,14,15]. Independent voltage-clamp measurements in internally dialyzed squid axons demonstrated voltage-dependent transport by the pump, extending the evidence beyond cardiac myocytes [7].

High-speed measurements resolved fast, intermediate, and slow $Na^+$-associated charge components, which describe ensemble relaxations rather than three isolated single-ion peaks. Their amplitudes and time courses depend on initial state occupancy, voltage, and extracellular $Na^+$; interpreting them as sequential release events therefore requires a kinetic scheme [13,18]. Charge-pulse experiments in reconstituted or purified pump preparations provide independent evidence that $Na^+$-transport reactions are electrogenic [38]. Section 5 distinguishes the observables and protocols used in these approaches.

$Na^+$-bound structures resolve coordination environments relevant to binding and occlusion [22,23]. Turnover-state cryo-EM adds a $[Na_3]$E2P intermediate preceding release and an outward-open E2P state [19]. These are structural observations; assigning a particular transition between them to a slow, intermediate, or fast electrical component remains a hypothesis unless tested under matched functional conditions.

Under the experimental conditions and kinetic interpretation of Castillo et al. [17], $K^+$-associated transients support two voltage-dependent extracellular binding reactions followed by a largely voltage-insensitive occlusion step. Their fitted electrical fractions and rates are summarized in Table 1. These effective coefficients are model- and protocol-dependent, not geometric distances read directly from a structure.

**Table 1.** Selected quantitative electrophysiological evidence for voltage-dependent pump function.

| Study and Preparation | Key Conditions and Protocol | Main Quantitative Result | Main Limitation |
| --- | --- | --- | --- |
| Stanley et al. [39] Human α2β1/α2β2 expressed in Xenopus oocytes | $Na^+$-loaded oocytes; extracellular $Na^+$ 150 mM and $K^+$ 4.5 mM; two-electrode voltage clamp | $K^+$-activated pump current was inhibited by approximately 75% in α2β1 and 95% in α2β2 at negative potentials | Results are protocol-specific and may not represent native cardiac complexes |
| Castillo et al. [17] Native Dosidicus gigas giant axon | $Na^+$-free $K^+/K^+$ exchange; 1–8 mM extracellular $K^+$; voltage steps from −140 to +80 mV | Fitted electrical fractions: $\lambda_1 = 0.46$ and $\lambda_2 = 0.27$; occlusion and deocclusion rates were approximately 13,450 and 2170 $s^{-1}$, respectively | Parameters are conditional on the kinetic model and experimental conditions |
| Colina et al. [40] Edited and unedited squid $Na^+/K^+$-ATPase expressed in Xenopus oocytes | Cut-open oocyte voltage clamp; ouabain-sensitive normalized current | I877V shifted the normalized I–V relation by approximately 25 mV toward more negative potentials | The shift does not uniquely identify a change in electrical distance or a specific microscopic rate |
| Gadsby et al. [18] Native Loligo pealei giant axon | $K^+$-free $Na^+$ branch; extracellular $Na^+$ 25–400 mM; voltage-jump protocol | At 25 mM extracellular $Na^+$, intermediate and fast charge components were approximately 7 ± 1% and 14 ± 1% of the maximal slow component | Component amplitudes depend on state occupancy, protocol, and temporal bandwidth |

Biochemical and spectroscopic studies indicate that ionic strength, divalent cations, and membrane-surface electrostatics can modulate conformational kinetics. Interactions involving the charged N-terminal region have been proposed as one possible contributor to this regulation [24–26,41]. Such observations do not establish an intrinsic E2-to-E1 voltage dependence without independently varying transmembrane potential. The rate-limiting transition may also change with experimental conditions. Reaction-based models of palytoxin-modified $Na^+/K^+$-ATPase have further illustrated how phosphorylation, ion binding, and $K^+$ occlusion can constrain the distribution of conformational states and the kinetics of experimentally observed currents [42,43].

*From Electrical Displacement to Microscopic Rate Changes*

The cycle-level thermodynamic constraint is established in Section 3; the present section concerns its kinetic allocation among microscopic transitions.

Voltage-sensitive transitions can be represented phenomenologically by assigning an effective electrical coefficient to the forward and reverse rates of a microscopic reaction. This coefficient describes how strongly the transition rate responds to membrane potential and should not automatically be interpreted as a literal geometric distance within the protein. Fitted values may combine ionic displacement, protein conformational changes, ligand binding, and redistribution among kinetic states [10,13,15,44].

For a reversible transition represented consistently with local thermodynamic constraints, the voltage dependence of the forward and reverse rates can be distributed differently between the two activation barriers. The rate ratio reflects the voltage-dependent state-energy difference, whereas the absolute rate magnitudes determine the relaxation timescale. Thus, two parameterizations may preserve the same equilibrium occupancy while predicting different transient kinetics [10,33,45].

In the $Na^+/K^+$-ATPase, this distinction is essential because steady-state current–voltage relations do not uniquely identify the electrical coefficient or activation barrier of any individual transition. Transient charge, relaxation kinetics, ligand dependence, and state occupancy must therefore be analyzed jointly when assigning voltage sensitivity to a microscopic step.

The concepts introduced here are formalized in Section 7, where state electrical coordinates, transition barriers, and effective rate coefficients are incorporated into thermodynamically consistent kinetic models.

## 5. Steady-State and Transient Electrophysiology

Steady-state current measures net electrogenic turnover after pump-state occupancies have reached a stationary distribution. Pre-steady-state transients measure voltage-induced redistribution among pump states with different electrical coordinates. Integration yields displaced charge $Q$, whereas the time course yields relaxation rates; neither observable is interchangeable with steady turnover or unidirectional ion flux [8,46,47]. Table 1 summarizes selected quantitative measurements, and Table 2 distinguishes structural observations from candidate electrophysiological assignments.

**Table 2.** Structural intermediates and candidate electrophysiological correspondences.

| Structural Intermediate | Candidate Transition or Observable | Evidence and Interpretation | Main Uncertainty |
|---|---|---|---|
| $Na^+$-bound E1 and occluded E1P-related states Kanai et al. [22]; Nyblom et al. [23] | $Na^+$ occlusion, E1P → E2P transition, and $Na^+$-associated transient charge | Ion-binding sites and conformational states resolved structurally; related electrical reactions measured independently | A one-to-one correspondence between a structural state and a relaxation component remains unestablished |
| $[Na_3]$E2P under turnover conditions Christensen et al. [19] | Pre-release rearrangement and extracellular $Na^+$ release; slow or intermediate $Na^+$-associated relaxation | Intermediate observed under turnover conditions and positioned within a candidate release pathway | No direct correspondence with a specific electrical component under matched voltage-clamp conditions |
| Outward-open E2P Christensen et al. [19] | Sequential extracellular $Na^+$ release/rebinding and three coupled $Na^+$ charge components | Structural state observed; sequential electrical components supported by kinetic analysis | Assigning individual charge components to specific structural transitions remains model-dependent |
| $K^+$-bound E2-related state Shinoda et al. [21] | External $K^+$ binding, occlusion, and $K^+$-associated Q–V and relaxation | Bound-ion structure and functional charge movements support two binding steps and weakly voltage-sensitive occlusion | Fitted electrical fractions and rates cannot be inferred directly from structure |

Q–V, charge–voltage relation.

In guinea pig ventricular myocytes, the steady-state $I_{pump}$–$V_m$ relation of the pump operating in the forward transport direction is strongly voltage dependent at negative potentials and approaches a plateau or shallow positive slope at more positive potentials under physiological extracellular $Na^+$ conditions [11]. Lowering extracellular $Na^+$ increases pump current preferentially at negative potentials and reduces the apparent voltage dependence, consistent with a contribution from extracellular $Na^+$ rebinding to the measured current–voltage relation [11,16]. Extracellular $K^+$ also modifies the $I_{pump}$–$V_m$ relation through interactions with outward-facing pump states, although the voltage dependence of the resulting response depends on the ionic conditions [16]. These measurements show

that steady-state current–voltage relations are conditional on extracellular ligands and state occupancy rather than being described by a single invariant voltage coefficient.

At low extracellular $K^+$, Xenopus oocytes can show a negative-slope region in the steady pump I–V relation [48]. This result illustrates that the sign and magnitude of apparent voltage sensitivity depend on the experimental conditions and cannot be treated as intrinsic, invariant properties of the enzyme.

Under conditions restricting turnover to the $Na^+/Na^+$ exchange branch, voltage jumps produce transient currents as pump states redistribute. The resulting charge displacement ($Q$) and relaxation rate coefficients reflect these conformational shifts, remaining distinct from unidirectional $Na^+$ flux [46,47]. An electroneutral $Na^+/Na^+$ exchange cycle can therefore exhibit voltage-dependent turnover without generating net stationary transport current, because charge movements during partial reactions can cancel over the complete exchange cycle [8,12]. Quantitative interpretation requires reporting the ionic and nucleotide conditions and the voltage protocol, including intracellular and extracellular $Na^+$, the presence or absence of $K^+$, ATP and ADP concentrations, holding potential, test potentials, and pulse duration [31,46,47].

Resolving multiple $Na^+$-associated components requires temporal resolution appropriate to their kinetics. The slow, intermediate, and fast signals depend on voltage, extracellular $Na^+$, and the state distribution established by the holding conditions. An apparent loss of a component may therefore reflect limited bandwidth or inaccessible occupancy rather than absence of the underlying transition. Models should reproduce component amplitudes and relaxation kinetics across protocols rather than only a single fitted time constant [13,18,20].

Charge-pulse and voltage-sensitive fluorescence approaches provide complementary measurements in purified or reconstituted membrane systems. Charge-pulse experiments with $Na^+/K^+$-ATPase fragments adsorbed to planar lipid bilayers measured voltage-dependent charge movements in the $Na^+$-transport pathway [38]. In the Albers–Post kinetic model used to interpret these data, the E1P → E2P transition was electrogenic but contributed relatively little charge, whereas the first extracellular $Na^+$-release step accounted for the largest charge displacement and subsequent release steps had smaller effective dielectric coefficients. These assignments are therefore model-dependent rather than direct observations of individual molecular transitions.

Capacitive-coupling approaches, including the SURFE2R methodology, provide an additional route for detecting electrogenic events from membrane pumps and transporters. These recordings are valuable for monitoring transport-associated charge movements in supported-membrane preparations, but their signals depend on membrane adsorption, orientation, capacitive coupling, and experimental configuration; they therefore complement rather than replace voltage-clamp measurements [49].

RH421 fluorescence complements electrical measurements but reports changes in the local probe environment rather than an exclusive measure of transmembrane charge displacement. Its response may reflect E1/E2 conformational changes and interactions involving charged protein regions and the membrane surface [25,50]. Ionic strength, divalent ions, and protein–lipid interactions must therefore be controlled before a fluorescence change is attributed to an intrinsic voltage-dependent transport step. Fairuz et al. [26] further identified electrostatic modulation of the E2 → E1 transition and proposed the lysine-rich N-terminal region as a likely contributor, but this assignment remains mechanistic rather than a direct demonstration of N-terminal causality.

Together, these approaches constrain complementary aspects of pump function: electrical recordings quantify current and charge redistribution, biochemical measurements constrain reaction rates, and structural studies identify conformations and ion-coordination environments. No single approach determines the complete voltage-dependent cycle.

## 6. Isoform-Specific Voltage Dependence

$Na^+/K^+$-ATPase isoforms differ in ion affinity, turnover, expression, and regulation. α1 is broadly distributed, α2 is prominent in muscle, and α3 is enriched in neurons [51]. Consequently, voltage responses should be attributed to a defined αβFXYD—which incorporates a regulatory subunity family (FXYD)—complex under specified experimental conditions rather than to the canonical 3:2 stoichiometry alone.

In Xenopus oocytes expressing human isoforms, Crambert et al. [52] reported, under the conditions examined, an apparent voltage-dependence order of α2 > α1 > α3. The same study showed that α/β pairing altered extracellular $K^+$ activation, with particularly low apparent $K^+$ affinity for α2β2. Horisberger and Kharoubi-Hess [53] likewise reported functional differences among rat α1, α2, and α3 pumps, including differences in extracellular cation dependence and cation-binding properties. These findings indicate that voltage sensitivity is an isoform-dependent phenotype emerging from the molecular reaction cycle rather than a universal consequence of 3:2 transport stoichiometry.

The physiological relevance of α/β-subunit composition is supported by experiments showing that astrocyte-associated α2β2 pumps display extracellular $K^+$ affinity and voltage dependence consistent with recruitment during neuronal activity [54]. These observations connect isoform-specific electrophysiological properties to a defined physiological function, without implying that ligand-dependent recruitment and intrinsic voltage sensitivity are equivalent.

Stanley et al. [39] reported stronger inhibition of recombinant α2β2 than α2β1 at negative potentials after correction for endogenous oocyte currents. Because these estimates depend on the normalization and voltage protocol, they should not be interpreted as universal inhibition fractions in native myocardium (Table 1). The physiological implications are considered in Section 8.

α3-containing pumps have relatively low apparent cytoplasmic $Na^+$ affinity, favoring recruitment during $Na^+$ loading [52]. Turnover structures of α1β1FXYD1 and α3β1FXYD1 provide candidate states for testing whether isoform differences alter electrical displacement or ligand-dependent occupancy [19]. Increased $Na^+$-dependent activity should not, by itself, be interpreted as direct voltage-dependent recruitment.

Comparisons among isoforms should therefore match α and β composition, FXYD expression, temperature, lipids, and ionic conditions before attributing a difference to intrinsic α-subunit voltage dependence.

*Post-Transcriptional Tuning of Voltage Dependence: RNA Editing in Cephalopods*

RNA editing provides a further source of functional diversity from a single $Na^+/K^+$-ATPase gene. Colina et al. [40] identified three recoding sites in squid $Na^+/K^+$-ATPase transcripts and found that their editing levels varied markedly and independently among tissues. More broadly, A-to-I RNA editing can modify proteins involved in neural excitability [55], and transcriptome-wide analyses have revealed extensive, tissue-dependent protein recoding in the squid nervous system, including ion-transport proteins [56]. However, tissue differences in editing levels do not, by themselves, demonstrate acute temporal regulation of pump voltage dependence.

Among the functionally characterized sites, the I877V substitution in transmembrane segment 7 shifted the normalized pump $I_{pump}$–$V_m$ relation by approximately 25 mV toward more negative potentials under the conditions studied, thereby reducing voltage-dependent inhibition over the corresponding voltage range [40].

For the I877V construct, the electrical depth of the extracellular access pathway was fixed at 0.67 because the current–voltage data did not reach saturation. The study therefore did not provide a free-parameter statistical comparison showing that electrical depth was

unchanged. The result should be described as a shift in voltage-dependent pump behavior, not as evidence that RNA editing changes the effective electrical distance [40].

This example illustrates the distinction between a shift in the observed $I_{pump}$–$V_m$ relation and a change in effective electrical distance. Discriminating between these possibilities requires charge–voltage measurements, relaxation kinetics, and ligand-dependence analyses in addition to steady-state pump current.

## 7. Kinetic Models of Voltage-Dependent Pump Function

Models of $Na^+/K^+$-ATPase voltage dependence range from algebraic current laws to explicit Albers–Post state networks. Algebraic formulations can efficiently reproduce steady-state current–voltage behavior within calibrated conditions, whereas state-based models represent occupancies and partial reactions at the cost of additional parameters. Their suitability depends on the intended observable, such as steady current, transient charge movement, metabolic response, or reversal [9,10,29]. These approaches are complementary rather than mutually exclusive.

Smith and Crampin [10] reduced a detailed 15-state transport scheme to four states using rapid-equilibrium assumptions while preserving thermodynamic constraints. Such a reduction is justified when the eliminated reactions remain sufficiently fast over the domain of interest, but it does not automatically preserve every experimentally resolvable relaxation.

Terkildsen et al. [34] applied a reduced cardiac pump formulation to ischemic extracellular $K^+$ accumulation. Pan et al. [28] subsequently identified and corrected inconsistencies in the equations and parameterization, reparametrized the model, and provided MATLAB (R2026b (version 26.2)), CellML, and bond-graph implementations. This history illustrates why agreement within a calibration range must be distinguished from thermodynamic consistency and reproducibility outside that range.

Guerra et al. [47] developed a 20-state multiscale framework incorporating structural intermediates, thermodynamic constraints, and incremental displacement charges. This framework provides a useful comparator for evaluating how structural, thermodynamic, and electrophysiological constraints are integrated in kinetic models.

For extrapolation across ionic gradients, ATP-hydrolysis free energy, or reversal, models should satisfy the cycle-level thermodynamic constraint established in Section 3. When transient behavior is an intended target, the retained states should be tested against Q–V relations and relaxation kinetics at the relevant temporal bandwidth. Isoform comparisons additionally require matched α- and β-subunit composition, FXYD association, temperature, and ionic conditions.

Model evaluation should be matched to the intended observable. Steady-state I–V measurements constrain net pump current under defined ionic and metabolic conditions but do not uniquely identify microscopic transitions. Transient charge measurements provide information about state redistribution and relaxation kinetics, whereas structural studies define ion-coordination environments and conformational states without directly determining rates or electrical distances. Mutagenesis, RNA editing, and isoform comparisons can reveal functional effects of specific molecular changes, but these effects may involve altered ligand binding, state occupancy, turnover, or voltage-dependent transitions. Cellular measurements additionally incorporate subunit composition, regulatory proteins, membrane environment, and endogenous currents.

Complementary stochastic approaches have been applied to palytoxin-induced $Na^+/K^+$-ATPase channels, using statistical model checking to investigate state-transition dynamics, reproduce experimental protocols, and evaluate mechanistic hypotheses, including a proposed diprotomeric organization [57]. Although these models describe toxin-modified

pumps rather than the native transport cycle, they illustrate how kinetic schemes can be constrained by electrophysiological observations.

Evaluation should report the calibration data, independent tests where available, parameter uncertainty, and the conditions over which predictions remain credible. Additional states or voltage-sensitive parameters are justified by improved prediction of the target observations, not merely by a closer fit to a single dataset. Section 9 formulates experiments and model comparisons that can challenge these assignments.

*Bond-Graph Formulations and Constitutive Thermodynamic Modeling*

Section 4 introduced the kinetic interpretation of electrical displacement. This section formalizes that interpretation sufficiently to distinguish the thermodynamic constraints of the complete cycle from the kinetic properties of individual transitions.

Bond-graph formulations combine chemical and electrical potentials with stoichiometric coupling and dissipative reaction elements [27]. They provide a framework for enforcing energetic consistency, but they do not determine the constitutive kinetic law. An explicit state model can therefore also be formulated as a bond-graph model [28].

For an ion of valence $z$ in compartment $k$, the molar electrochemical potential is

$$\mu_{z,k} = \mu_{z,k}^{\circ} + RT \ln a_{z,k} + zF\psi_k, \tag{6}$$

where $a_{z,k}$ is the dimensionless activity and $\psi_k$ is the electrical potential. Internal pump states can be assigned corresponding chemical and electrical potentials. The electrical contribution of an internal state may be represented by a molar coordinate $q_i$, expressed in C.mol$^{-1}$, so that the state potential includes a term $q_i V_m$. The quantity $q_i$ is a model coordinate and should not automatically be interpreted as the displacement of a literal elementary charge.

The free energy of an individual pump state depends on the chosen chemical and electrical reference. For ligand-coupled reactions, however, the state-energy difference is insufficient because the electrochemical potentials of exchanged ligands must also be included. With the forward direction defined consistently, the molar reaction free-energy change is the total potential of products minus that of reactants, whereas the forward reaction affinity is its negative. These definitions distinguish state energies, reaction energetics, and the driving force for net flux.

For a reversible reaction r, the forward and reverse reaction potentials must include all participating pump states and chemostatted ligands. The reaction affinity is determined by their difference:

$$A_r = \mu_{r,\mathrm{f}} - \mu_{r,\mathrm{r}}, \tag{7}$$

where $\mu_{r,\mathrm{f}}$ and $\mu_{r,\mathrm{r}}$ denote the total forward and reverse reaction potentials. For ion-binding or transport reactions, the corresponding reservoir terms must be included explicitly; for a pure conformational isomerization, no additional ligand term is required [9,27].

When the reaction affinities are summed around a complete forward cycle, the internal-state potentials cancel. The remaining terms are determined by the chemical and electrical potentials of the external reservoirs:

$$A_{\mathrm{cycle}} = \sum_r A_r = -\Delta G_{\mathrm{cycle}}, \tag{8}$$

with the sign convention used in Section 3. Thus, the affinity of the complete cycle is determined by transport stoichiometry, ion activities, nucleotide conditions, and membrane potential. A closed conformational loop that is not coupled to ionic or chemical reservoirs cannot generate the non-zero free-energy change associated with net electrogenic transport [9,33]. Here, the cycle free-energy change is the forward products-minus-reactants

quantity, so the cycle affinity is its negative; this is the same sign convention as in Section 3, where negative forward-cycle free energy favors forward transport.

For a microscopic transition between states i and j, define $\Delta G^{o}_{eff,ij}(V_m)$ as the transformed standard molar free-energy difference for the specified forward reaction, including any fixed chemostatted ligand activities and electrical terms, but excluding the instantaneous ratio of state occupancies. Its value depends on the stated reference and reservoir conditions. The actual reaction free-energy change additionally contains the population-dependent contribution $RTln\left(\frac{p_j}{p_i}\right)$ for an ideal two-state description; correspondingly, the instantaneous affinity is not generally zero in a driven or relaxing system.

The thermodynamic constraint of the complete cycle does not uniquely determine the forward and reverse kinetic coefficients of every microscopic transition. For an elementary reversible isomerization, local detailed balance fixes the ratio of the forward and reverse first-order rate constants through the corresponding transformed standard reaction free energy. For ligand-association steps, intrinsic association constants and dissociation constants have different units; the dimensionally comparable quantities are effective pseudo-first-order rates obtained after multiplying the association constants by the appropriate ligand activities or concentrations. Such effective rates must be defined under specified chemostatted conditions. In either case, the rate ratio constrains the reversible thermodynamic bias, whereas the common kinetic scale depends on activation barriers or constitutive mobility. In simplified form,

$$\frac{k_{ij}(V_m)}{k_{ji}(V_m)} = \exp\left[-\frac{\Delta G^{o}_{eff,ij}(V_m)}{RT}\right]. \tag{9}$$

In Equation (9), $\Delta G^{o}_{eff,ij}(V_m)$ denotes the transformed standard free-energy difference just defined, and $k_{ij}$ and $k_{ji}$ denote dimensionally matched first-order rates at fixed reservoir conditions. The equation is a local detailed-balance relation, not an assertion that the actual reaction affinity vanishes during turnover. It determines the equilibrium occupancy ratio of an isolated reversible two-state subsystem, but not its relaxation time. In a multistate pump operating away from equilibrium, stationary occupancies and currents depend on the complete network of rates and cycle affinities; preserving individual forward/reverse ratios alone need not preserve those nonequilibrium observables. The voltage dependence of the rate ratio and of the common kinetic scale are therefore related but distinct.

This distinction can be illustrated with a reversible two-state transition. At a fixed voltage, consider $i \rightleftharpoons j$ with $k^+ = 100\ s^{-1}$ and $k^- = 50\ s^{-1}$. Multiplying both rates by five gives $k^+ = 500\ s^{-1}$ and $k^- = 250\ s^{-1}$. The ratio remains two, so the equilibrium occupancy of state j remains

$$p_{j,eq} = \frac{k^+}{k^+ + k^-} = \frac{2}{3}, \tag{10}$$

but the relaxation time changes from approximately 6.67 ms to 1.33 ms. The two parameterizations therefore predict the same equilibrium occupancy and equilibrium charge but different transient time courses. This equivalence in equilibrium occupancy applies only to the isolated two-state example at fixed reservoir conditions and should not be generalized to a driven multistate stationary distribution.

In multistate $Na^+/K^+$-ATPase models, the electrical displacement assigned to a pathway can be distributed among several microscopic transitions. Within the framework of Guerra et al. [45], the total electrical displacement along a specified pathway can be expressed as the sum of the signed incremental displacements assigned to its transitions:

$$q_{path} = \sum_r \Delta q_r. \tag{11}$$

This relation constrains the total displacement but does not uniquely identify the contribution of each transition or its activation barrier. Thermodynamically consistent models

with different state-space resolutions may therefore share the same cycle affinity and reversal potential while predicting different transient charge movements and relaxation kinetics.

Greater structural resolution should therefore be treated as an additional constraint on model topology rather than as a direct measurement of electrical coefficients or transition rates. Discriminating among alternative parameterizations requires independent measurements of transient charge, relaxation kinetics, and ligand dependence in addition to steady-state current–voltage relations [10,28,47].

Energy-based models should therefore report their voltage and reservoir conventions, transport stoichiometry, state definitions, kinetic coefficients, calibration data, and independent validation tests. Thermodynamic consistency is necessary for extrapolation across ionic, metabolic, and voltage conditions, but it does not guarantee that a model will reproduce the transient or isoform-specific observables targeted by the analysis.

## 8. Physiological and Pathological Implications

Pump turnover, membrane potential, and ionic gradients form a coupled feedback system (Figure 3). The $Na^+/K^+$-ATPase generates outward electrogenic current and sustains the $Na^+$ and $K^+$ gradients that support neuronal firing, secondary active transport, and extracellular ionic homeostasis. Membrane voltage modifies the electrical work of transport and voltage-sensitive microscopic transitions, whereas activity-dependent changes in ion activities and ATP hydrolysis alter substrate availability, cycle affinity, and state occupancy. These contributions must be distinguished when extrapolating voltage-clamp measurements to intact neural tissue, in which they evolve together [28,30].

In intact cells, membrane potential is an emergent property determined by transmembrane ionic gradients and the relative permeability of the membrane to different ions. $K^+$ permeability is a major determinant of the resting potential, whereas voltage-gated and ligand-gated channels, ion exchangers, cotransporters, membrane capacitance, and external inputs contribute to dynamic changes in membrane voltage. The $Na^+/K^+$-ATPase contributes directly through its electrogenic 3:2 transport stoichiometry and indirectly by maintaining the $Na^+$ and $K^+$ gradients that establish the driving forces for other membrane transport pathways [6,28,30]. Therefore, membrane potential both regulates pump activity and is influenced by pump-mediated current and gradient maintenance. This physiological feedback differs from voltage-clamp experiments, in which membrane potential is imposed experimentally to assess voltage-dependent pump function.

In the brain, this coupling is distributed across neurons, astrocytes, and the restricted extracellular space. Neuronal $Na^+$ entry during firing increases the demand for extrusion, while extracellular $K^+$ accumulation requires coordinated clearance and redistribution. $Na^+/K^+$-ATPase isoforms are not interchangeable in this context. Cell-type-specific expression studies have identified α1 in both neuronal and glial populations, α3 predominantly in neurons, and α2 prominently in astrocytes, although the distributions overlap and vary across brain regions and preparations [58,59]. These expression patterns are accompanied by functional specialization: neuronal α3 supports recovery from activity-dependent $Na^+$ loading, whereas astrocytic α2-containing complexes contribute to extracellular $K^+$ clearance, with their recruitment depending on ion affinities, subunit composition, and membrane voltage [52,54,60]. These patterns support distinct functional recruitment regimes, but do not establish that voltage-dependent microscopic rate constants measured in one cellular environment apply unchanged to another.

Computational studies of nonsynaptic epileptiform activity illustrate the importance of electrogenic pump current within tissue-scale ionic feedback. Almeida et al. [6] proposed that burst onset and termination can be associated, respectively, with neuronal $Na^+$ influx exceeding pump-mediated outward current and with pump current again ex-

ceeding $Na^+$ influx. This is a model-derived mechanistic interpretation rather than direct experimental resolution of individual pump transitions. Computational studies of nonsynaptic epileptiform activity have also shown that extracellular $K^+$ accumulation and gap-junction-mediated interactions can jointly influence neuronal firing patterns and synchronization [61]. These findings reinforce the importance of considering $Na^+/K^+$-ATPase activity within a coupled tissue-level system rather than as an isolated membrane current. In hippocampal preparations with high extracellular $K^+$ and nominally $Ca^{2+}$-free perfusion, Rodrigues et al. [62] combined experiments and simulations to suggest that reduced extracellular $Mg^{2+}$ intensifies nonsynaptic discharges through both diminished surface-charge screening and reduced pump activity. These findings emphasize that changes in excitability cannot be attributed to intrinsic voltage sensitivity of the pump without independently accounting for ion activities and membrane-surface electrostatics.

The same distinction is important for spreading depression (SD). In an electrodiffusive tissue model, Teixeira et al. [63] associated SD refractoriness with coupled neuronal and glial recovery mechanisms and the redistribution of extracellular $K^+$. More recently, Rodrigues et al. [64] showed that a simplified excitable-media model reproduces spiral-wave dynamics and that partial inhibition of $Na^+/K^+$-ATPase by ouabain in avian retina reduced recovery and extinguished spiral activity. These experiments implicate pump-dependent recovery in the persistence of reentrant SD waves; they do not isolate voltage-dependent elementary reaction rates or identify which isoform mediates the effect. Thus, tissue-level recovery parameters should not be equated directly with molecular pump turnover or with a particular $k_{ij}(V_m)$.

$Na^+/K^+$-ATPase activity also supports other transport processes by maintaining their electrochemical driving forces. In computational simulations of nonsynaptic epileptiform activity, Rodrigues et al. [65] examined how fluctuations in $Na^+$, $K^+$, and $Cl^-$ interact with acid–base transport to generate changes in pH. In a separate spiking-network model, Ahmed et al. [66] found that learning performance depends on KCC2/NKCC1 transport parameters and on the assumed NKCC1 stoichiometry. These studies do not measure $Na^+/K^+$-ATPase voltage dependence directly; rather, they illustrate how pump-maintained gradients can influence pH regulation, chloride homeostasis, and network function through downstream transport mechanisms.

During ischemia, spreading depression, or prolonged epileptiform activity, depolarization and changes in $Na^+$ and $K^+$ activities alter the energetic cost of forward transport, whereas a less exergonic ATP-hydrolysis reaction reduces metabolic driving force. These thermodynamic contributions can act in opposing directions, and the resulting current also depends on ligand binding, microscopic kinetics, and state occupancy [28,34]. Neither ATP depletion nor a uniform direction of pump-current change should be presumed for every seizure or SD event. The central experimental challenge is to separate changes in pump abundance, isoform composition, substrate activities, and intrinsic voltage-sensitive transitions before assigning a tissue-level phenotype to a specific molecular mechanism.

*Isoform-Specific Recruitment and Physiological Specialization of $Na^+/K^+$-ATPase*

The distinct cellular distributions and apparent intracellular $Na^+$ affinities of α isoforms provide a mechanistic basis for heterogeneous pump recruitment. In many mature neurons, α3-containing pumps are positioned to contribute strongly when intracellular $Na^+$ rises during sustained or repetitive activity, whereas α1-containing pumps can support substantial activity under resting conditions. Astrocytes commonly express α1- and α2-containing pumps, and experimental evidence indicates that α2β2 complexes exhibit $K^+$ affinity and voltage-dependent behavior suited to recruitment during activity-dependent elevations of extracellular $K^+$ [54,59]. Experiments in neurons coexpressing α1 and α3 have

demonstrated a distinct contribution of α3-containing pumps to the recovery of intracellular $Na^+$ following neuronal activity, supporting a functional division between isoforms rather than simple redundancy [60]. These are functional tendencies rather than absolute cell-type markers: expression, localization, β-subunit association, and kinetic behavior depend on preparation and physiological context.

Isoform-specific recruitment should not be interpreted solely as a consequence of different apparent $Na^+$ or $K^+$ affinities. A depolarization-induced change in pump current at fixed ligand activities reflects a different experimental constraint from recruitment driven by changing $[Na^+]_i$ or $[K^+]_o$ in intact tissue. Furthermore, voltage-dependent redistribution among molecular states can interact with ligand availability and produce time-dependent responses. Assigning distinct voltage-sensitive rate constants to neuronal α3 and astrocytic α2 requires isoform-resolved measurements or appropriately constrained kinetic models; the cited tissue studies alone do not provide those constants.

The functional specialization of neuronal and astrocytic $Na^+/K^+$-ATPase isoforms suggests that their distinct kinetic properties, substrate affinities, and cellular localization may influence activity-dependent ionic recovery beyond differences in total pump capacity [52,53,60]. However, the relative contributions of isoform-specific kinetics and spatial distribution to tissue-level responses remain to be established, particularly for extracellular $K^+$ clearance, neuronal $Na^+$ recovery, and spreading-depression refractoriness [54,60,63]. A quantitative comparison of isoform-resolved and homogeneous pump models, designed to discriminate these contributions, is proposed in Section 9.

A cardiac example remains informative but secondary: α2-associated pumps in ventricular myocytes have been linked to local $Na^+$ regulation and $Na^+/Ca^{2+}$ exchange [39,67]. However, the physiological interpretation of these observations should not be transferred directly to astrocytic α2 or neuronal α3 without accounting for differences in cellular organization, ionic conditions, and kinetic context.

## 9. Predictions and Experimental Tests

The preceding analysis suggests a series of complementary tests to distinguish changes in pump abundance, ion-dependent state occupancy, microscopic electrical displacement, and intrinsic reaction kinetics. The central requirement is to compare mechanisms under controlled ionic and metabolic conditions while assessing more than one observable. In particular, steady-state current–voltage relations alone cannot uniquely identify voltage-sensitive elementary steps; transient charge–voltage relations, relaxation kinetics, and responses to ligand perturbations provide additional constraints [10,28].

A first test would separate changes in surface pump abundance from changes in intrinsic kinetics. For a fixed αβFXYD complex, surface expression could be varied and independently quantified while temperature, membrane composition, ionic and nucleotide activities, and voltage protocols are held as constant as practicable. If individual pumps retain the same kinetics and initial-state distributions, increasing their number should scale steady pump current and movable charge proportionally without changing normalized I–V or Q–V relations or relaxation time constants. Deviations from this prediction would indicate that an abundance-only description is insufficient, although altered maturation, membrane organization, or pump–pump interactions would need to be excluded before attributing the effect to intrinsic rate changes.

A second test would ask whether the different voltage responses of α isoforms require different microscopic electrical displacements or can be explained by altered ligand affinities, state occupancies, and rate-limiting transitions. Recombinant α1β1, α2β1, α2β2, and α3β1 complexes could be compared across matched $Na^+$ and $K^+$ conditions, with FXYD association, temperature, nucleotide activities, and surface expression controlled. Joint

fitting of steady I–V relations, Q–V distributions, and relaxation time courses could then compare thermodynamically constrained models that either share or allow isoform-specific state-to-state electrical coefficients. Accurate predictions for withheld conditions using shared coefficients would show that distinct electrical displacements are not required by the available data, whereas persistent discrepancies resolved by identifiable coefficient differences would favor isoform-dependent electrical allocation. A change in Q–V slope alone would not discriminate these mechanisms, because multistate occupancy also shapes the measured relation [39,52].

At the tissue scale, a third test would evaluate whether explicit isoform-specific recruitment improves predictions of activity-dependent ionic recovery. Spatially resolved neuron–astrocyte models containing separate α1, α2, and α3 pump populations could be compared with models using homogeneous pump kinetics but matched total pump capacity. Both descriptions should preserve canonical transport stoichiometry and cycle-level thermodynamic constraints and should be tested under the same ionic and metabolic conditions, with pump abundance and localization constrained independently wherever possible. Relevant observables include extracellular $K^+$ clearance, neuronal $Na^+$ recovery, post-activity excitability, and spreading-depression refractoriness. Experimental evidence for neuronal α3-dependent $Na^+$ recovery and astrocytic pump contributions to $K^+$ clearance motivates this comparison, while previous tissue models provide physiological targets rather than direct measurements of isoform-specific voltage-sensitive rates [54,60,63]. Superior predictions across independent conditions would support the value of isoform resolution; comparable performance would indicate that the added complexity is not yet warranted by the available observations.

A fourth test would seek a functional assignment for the $Na^+$-bound structural intermediates identified under turnover conditions. In particular, a transition involving $[Na_3]$E2P could be hypothesized to contribute to a specified $Na^+$-associated relaxation component [19]. Residues predicted to influence the stability of this intermediate could be perturbed, with catalytic competence, expression, ion affinities, and ionic conditions assessed independently. Voltage-jump currents, Q–V distributions, and relaxation time constants should then be compared with quantitative predictions defined in advance by a kinetic scheme. A selective, reproducible change matching the predicted component would strengthen the proposed correspondence; broad impairment of transport or changes incompatible with the scheme would weaken it. Because mutations may alter several transitions and state occupancies, a change in pump current alone cannot establish a one-to-one correspondence between a structural intermediate and an electrical relaxation component.

A fifth test would distinguish modulation by membrane-surface electrostatics from direct sensitivity to transmembrane voltage. Membrane surface charge or divalent-ion conditions could be varied while $V_m$ is controlled independently and free ion and nucleotide activities, including MgATP speciation, are monitored as closely as possible. Combined measurements of conformational kinetics and electrical responses could assess whether E2 → E1 kinetics change under altered surface conditions after accounting for ligand binding and the local electrostatic environment. Such a result would support a contribution from surface electrostatics without excluding additional intrinsic voltage sensitivity. Conversely, reproducible voltage-dependent kinetics under appropriately matched surface and ligand conditions would support a direct voltage-sensitive component. Because ionic-strength manipulations can simultaneously affect ligand activity, screening, and protein conformation, their effects must be interpreted with an explicit mechanistic model rather than assigned to a single cause [25,26].

Finally, alternative allocations of voltage-sensitive activation barriers should be evaluated by their ability to predict data not used for calibration. Competing state-based schemes

could be fitted to the same steady I–V dataset while preserving transport stoichiometry, reservoir conventions, and cycle thermodynamics. Their predictions for withheld Q–V curves, relaxation kinetics, and ligand-perturbation protocols would then be compared alongside parameter uncertainty, sensitivity, and practical identifiability. Failure of one fitted parameter set would challenge that parameterization but would not by itself invalidate the entire model structure; rejection of the latter would require showing that no admissible parameterization adequately accounts for the independent observations. If alternative schemes remain observationally indistinguishable, that limitation should be reported rather than interpreted as unique identification of microscopic rates [10,28].

Together, these tests link molecular and cellular observations without assuming that agreement with a single current–voltage curve establishes mechanism. Their purpose is to identify which distinctions are experimentally resolvable, reject unsupported assignments, and define the conditions under which a model is predictive. Additional states or isoform-specific kinetic parameters are justified when they improve independent predictions at the relevant temporal and spatial scales while remaining consistent with the thermodynamics of the complete transport cycle.

## 10. Concluding Remarks and Future Perspectives

The review shows that net electrogenicity, cycle-level thermodynamics, and microscopic voltage-sensitive kinetics are distinct but coupled aspects of $Na^+/K^+$-ATPase function. Structural, electrophysiological, and isoform-specific evidence provides complementary constraints, but no single approach independently identifies microscopic rate constants. Predictive models should therefore be tested against multiple observables and independent experimental conditions while preserving the thermodynamic consistency of the complete transport cycle.

Two priorities follow: mapping defined structural transitions onto measured charge and relaxation components, and determining whether isoform-specific voltage-dependent recruitment reflects electrical displacement, ligand-dependent occupancy, or both. Addressing these gaps requires matched subunit composition and conditions, joint electrical and structural constraints, and explicit uncertainty. Experiments should specify the causal direction being tested; models should preserve cycle energetics and retain only the kinetic detail supported by their intended measurements.

**Author Contributions:** Conceptualization, P.R.V.M. and A.M.R.; methodology, P.R.V.M., A.M.R. and A.-C.G.d.A.; validation, A.M.R. and A.-C.G.d.A.; investigation, P.R.V.M., A.C.P. and A.M.R.; resources, A.-C.G.d.A., A.M.R., F.A.S. and C.A.S.; writing—original draft preparation, P.R.V.M., A.M.R., A.-C.G.d.A., A.C.P.; writing—review and editing, A.-C.G.d.A., C.A.S., F.A.S. and A.M.R.; visualization, P.R.V.M., A.C.P. and A.M.R.; supervision, A.M.R. and A.-C.G.d.A. All authors have read and agreed to the published version of the manuscript.

**Funding:** This work was supported by Fundação de Amparo à Pesquisa do Estado de Minas Gerais (FAPEMIG), Fundação de Amparo à Pesquisa do Estado de São Paulo (FAPESP), Conselho Nacional de Desenvolvimento Científico e Tecnológico (CNPq), Financiadora de Estudos e Projetos (FINEP), and Coordenação de Aperfeiçoamento de Pessoal de Nível Superior (CAPES/PROEX), grant number 88881.844786/2023-01.

**Institutional Review Board Statement:** Not applicable.

**Informed Consent Statement:** Not applicable.

**Data Availability Statement:** No new data were created or analyzed in this study. Data sharing is not applicable to this article.

**Conflicts of Interest:** The authors declare no conflicts of interest.

## References


1. Skou, J.C. The influence of some cations on an adenosine triphosphatase from peripheral nerves. *Biochim. Biophys. Acta* **1957**, *23*, 394–401. [CrossRef]
2. Kaplan, J.H. Biochemistry of Na,K-ATPase. *Annu. Rev. Biochem.* **2002**, *71*, 511–535. [CrossRef]
3. Albers, R.W. Biochemical aspects of active transport. *Annu. Rev. Biochem.* **1967**, *36*, 727–756. [CrossRef]
4. Post, R.L.; Kume, S.; Tobin, T.; Orcutt, B.; Sen, A.K. Flexibility of an active center in sodium-plus-potassium adenosine triphosphatase. *J. Gen. Physiol.* **1969**, *54*, 306–326. [CrossRef]
5. Gadsby, D.C.; Kimura, J.; Noma, A. Voltage dependence of Na/K pump current in isolated heart cells. *Nature* **1985**, *315*, 63–65. [CrossRef]
6. Almeida, A.C.G.; Rodrigues, A.M.; Scorza, F.A.; Cavalheiro, E.A.; Teixeira, H.Z.; Duarte, M.A.; Silveira, G.A.; Arruda, E.Z. Mechanistic hypotheses for nonsynaptic epileptiform activity induction and its transition from the interictal to ictal state—Computational simulation. *Epilepsia* **2008**, *49*, 1908–1924. [CrossRef]
7. Rakowski, R.F.; Gadsby, D.C.; De Weer, P. Stoichiometry and voltage dependence of the sodium pump in voltage-clamped, internally dialyzed squid giant axon. *J. Gen. Physiol.* **1989**, *93*, 903–941. [CrossRef]
8. Rakowski, R.F.; Gadsby, D.C.; de Weer, P. Voltage dependence of the Na/K pump. *J. Membr. Biol.* **1997**, *155*, 105–112. [CrossRef]
9. Läuger, P. Thermodynamic and kinetic properties of electrogenic ion pumps. *Biochim. Biophys. Acta* **1984**, *779*, 307–341. [CrossRef]
10. Smith, N.P.; Crampin, E.J. Development of models of active ion transport for whole-cell modelling: Cardiac sodium-potassium pump as a case study. *Prog. Biophys. Mol. Biol.* **2004**, *85*, 387–405. [CrossRef]
11. Gadsby, D.C.; Nakao, M. Steady-state current-voltage relationship of the Na/K pump in guinea pig ventricular myocytes. *J. Gen. Physiol.* **1989**, *94*, 511–537. [CrossRef]
12. Gadsby, D.C.; Rakowski, R.F.; De Weer, P. Extracellular access to the Na,K pump: Pathway similar to ion channel. *Science* **1993**, *260*, 100–103. [CrossRef]
13. Holmgren, M.; Wagg, J.; Bezanilla, F.; Rakowski, R.F.; De Weer, P.; Gadsby, D.C. Three distinct and sequential steps in the release of sodium ions by the $Na^+/K^+$-ATPase. *Nature* **2000**, *403*, 898–901. [CrossRef]
14. Läuger, P.; Apell, H.J. A microscopic model for the current-voltage behaviour of the Na,K-pump. *Eur. Biophys. J.* **1986**, *13*, 309–321. [CrossRef]
15. Läuger, P.; Apell, H.J. Transient behaviour of the $Na^+/K^+$-pump: Microscopic analysis of nonstationary ion-translocation. *Biochim. Biophys. Acta* **1988**, *944*, 451–464. [CrossRef]
16. Nakao, M.; Gadsby, D.C. [Na] and [K] dependence of the Na/K pump current-voltage relationship in guinea pig ventricular myocytes. *J. Gen. Physiol.* **1989**, *94*, 539–565. [CrossRef]
17. Castillo, J.P.; Rui, H.; Basilio, D.; Das, A.; Roux, B.; Latorre, R.; Bezanilla, F.; Holmgren, M. Mechanism of potassium ion uptake by the $Na^+/K^+$-ATPase. *Nat. Commun.* **2015**, *6*, 7622. [CrossRef]
18. Gadsby, D.C.; Bezanilla, F.; Rakowski, R.F.; De Weer, P.; Holmgren, M. The dynamic relationships between the three events that release individual $Na^+$ ions from the $Na^+/K^+$-ATPase. *Nat. Commun.* **2012**, *3*, 669. [CrossRef]
19. Christensen, M.E.; Habeck, M.; Katz, A.; Fruergaard, M.U.; Peleg, Y.; Pick, U.; Karlish, S.J.D.; Nissen, P. Active conformations of neuronal $Na^+$,$K^+$-ATPase isoforms and a disease-causing mutant. *Nat. Commun.* **2026**, *17*, 9278. [CrossRef]
20. Hilgemann, D.W. Channel-like function of the Na,K pump probed at microsecond resolution in giant membrane patches. *Science* **1994**, *263*, 1429–1432. [CrossRef]
21. Shinoda, T.; Ogawa, H.; Cornelius, F.; Toyoshima, C. Crystal structure of the sodium–potassium pump at 2.4 Å resolution. *Nature* **2009**, *459*, 446–450. [CrossRef]
22. Kanai, R.; Ogawa, H.; Vilsen, B.; Cornelius, F.; Toyoshima, C. Crystal structure of a $Na^+$-bound $Na^+$,$K^+$-ATPase preceding the E1P state. *Nature* **2013**, *502*, 201–206. [CrossRef]
23. Nyblom, M.; Poulsen, H.; Gourdon, P.; Reinhard, L.; Andersson, M.; Lindahl, E.; Fedosova, N.; Nissen, P. Crystal structure of $Na^+$,$K^+$-ATPase in the Na+-bound state. *Science* **2013**, *342*, 123–127. [CrossRef]
24. Humphrey, P.A.; Lüpfert, C.; Apell, H.J.; Cornelius, F.; Clarke, R.J. Mechanism of the rate-determining step of the $Na^+$,$K^+$-ATPase pump cycle. *Biochemistry* **2002**, *41*, 9496–9507. [CrossRef]
25. Garcia, A.; Pratap, P.R.; Lüpfert, C.; Cornelius, F.; Jacquemin, D.; Lev, B.; Allen, T.W.; Clarke, R.J. The voltage-sensitive dye RH421 detects a $Na^+$,$K^+$-ATPase conformational change at the membrane surface. *Biochim. Biophys. Acta Biomembr.* **2017**, *1859*, 813–823. [CrossRef]
26. Fairuz, S.; Li, Z.; Gorman, A.; Cornelius, F.; Clarke, R.J. Electrostatic interaction as a key modulator of $Na^+$,$K^+$-ATPase function. *J. Membr. Biol.* **2026**, *259*, 17. [CrossRef]
27. Gawthrop, P.J.; Cursons, J.; Crampin, E.J. Hierarchical bond graph modelling of biochemical networks. *Proc. R. Soc. A* **2015**, *471*, 20150642. [CrossRef]
28. Pan, M.; Gawthrop, P.J.; Cursons, J.; Tran, K.; Crampin, E.J. The cardiac $Na^+/K^+$ ATPase: An updated, thermodynamically consistent model. *Physiome* **2020**, 1–14. [CrossRef]

29. Apell, H.J. Electrogenic properties of the Na,K pump. *J. Membr. Biol.* **1989**, *110*, 103–114. [CrossRef]
30. Glitsch, H.G. Electrophysiology of the sodium-potassium-ATPase in cardiac cells. *Physiol. Rev.* **2001**, *81*, 1791–1826. [CrossRef]
31. Moreno, C.; Yano, S.; Bezanilla, F.; Latorre, R.; Holmgren, M. Transient electrical currents mediated by the $Na^+/K^+$-ATPase: A tour from basic biophysics to human diseases. *Biophys. J.* **2020**, *119*, 236–242. [CrossRef]
32. Sidhu, R.K.; Maparu, K.; Singh, S.; Aran, K.R. Unveiling the role of $Na^+/K^+$-ATPase pump: Neurodegenerative mechanisms and therapeutic horizons. *Pharmacol. Rep.* **2025**, *77*, 576–592. [CrossRef]
33. Hill, T.L. *Free Energy Transduction and Biochemical Cycle Kinetics*; Springer: New York, NY, USA, 1989. [CrossRef]
34. Terkildsen, J.R.; Crampin, E.J.; Smith, N.P. The balance between inactivation and activation of the $Na^+$-$K^+$ pump underlies the triphasic accumulation of extracellular $K^+$ during myocardial ischemia. *Am. J. Physiol. Heart Circ. Physiol.* **2007**, *293*, H3036–H3045. [CrossRef]
35. Kravtsova, V.V.; Fedorova, A.A.; Matytsin, V.O.; Ganke, D.D.; Vetrovoy, O.V.; Krivoi, I.I. Short-term simulated high-altitude hypoxia enhances Na,K-ATPase efficiency in maintaining rat diaphragm electrogenesis. *Bull. Exp. Biol. Med.* **2025**, *179*, 756–761. [CrossRef]
36. Clarke, R.J.; Catauro, M.; Rasmussen, H.H.; Apell, H.-J. Quantitative calculation of the role of the $Na^+$,$K^+$-ATPase in thermogenesis. *Biochim. Biophys. Acta* **2013**, *1827*, 1205–1212. [CrossRef]
37. Nakao, M.; Gadsby, D.C. Voltage dependence of Na translocation by the Na/K pump. *Nature* **1986**, *323*, 628–630. [CrossRef]
38. Wuddel, I.; Apell, H.J. Electrogenicity of the sodium transport pathway in the Na,K-ATPase probed by charge-pulse experiments. *Biophys. J.* **1995**, *69*, 909–921. [CrossRef]
39. Stanley, C.M.; Gagnon, D.G.; Bernal, A.; Meyer, D.J.; Rosenthal, J.J.; Artigas, P. Importance of the voltage dependence of cardiac Na/K ATPase isozymes. *Biophys. J.* **2015**, *109*, 1852–1862. [CrossRef]
40. Colina, C.; Palavicini, J.P.; Srikumar, D.; Holmgren, M.; Rosenthal, J.J.C. Regulation of $Na^+/K^+$ ATPase transport velocity by RNA editing. *PLoS Biol.* **2010**, *8*, e1000540. [CrossRef]
41. Chkadua, G.; Nozadze, E.; Tsakadze, L.; Shioshvili, L.; Leladze, M.; Arutinova, N.; Dzneladze, S.; Javakhishvili, M.; Jariashvili, T. Cytochrome c and ouabain binding site of Na,K-ATPase. *Cell Biochem. Biophys.* **2025**, *83*, 2627–2635. [CrossRef]
42. Rodrigues, A.M.; Almeida, A.C.G.; Infantosi, A.F.C. Effect of palytoxin on the sodium–potassium pump: Model and simulation. *Phys. Biol.* **2008**, *5*, 036005. [CrossRef]
43. Rodrigues, A.M.; Infantosi, A.F.C.; de Almeida, A.C.G. Palytoxin and the sodium/potassium pump—Phosphorylation and potassium interaction. *Phys. Biol.* **2009**, *6*, 036010. [CrossRef]
44. Sagar, A.; Rakowski, R.F. Access channel model for the voltage dependence of the forward-running $Na^+/K^+$ pump. *J. Gen. Physiol.* **1994**, *103*, 869–893. [CrossRef]
45. Guerra, J.; Rui, H.; Roux, B. Multistate kinetic model of the sodium–potassium ATPase. *J. Phys. Chem. B* **2025**, *129*, 9609–9621. [CrossRef]
46. Holmgren, M.; Rakowski, R.F. Pre-steady-state transient currents mediated by the Na/K pump in internally perfused Xenopus oocytes. *Biophys. J.* **1994**, *66*, 912–922. [CrossRef]
47. Holmgren, M.; Rakowski, R.F. Charge translocation by the $Na^+/K^+$ pump under $Na^+/Na^+$ exchange conditions: Intracellular Na+ dependence. *Biophys. J.* **2006**, *90*, 1607–1616. [CrossRef]
48. Rakowski, R.F.; Vasilets, L.A.; LaTona, J.; Schwarz, W. A negative slope in the current-voltage relationship of the $Na^+/K^+$ pump in Xenopus oocytes produced by reduction of external $[K^+]$. *J. Membr. Biol.* **1991**, *121*, 177–187. [CrossRef]
49. Clarke, R.J. The SURFE2R surface electrogenic event reader: From fundamental research to commercial product. *Biophys. Rev.* **2025**, *17*, 809–827. [CrossRef]
50. Heyse, S.; Wuddel, I.; Apell, H.J.; Stürmer, W. Partial reactions of the Na,K-ATPase: Determination of rate constants. *J. Gen. Physiol.* **1994**, *104*, 197–240. [CrossRef]
51. Blanco, G.; Mercer, R.W. Isozymes of the Na-K-ATPase: Heterogeneity in structure, diversity in function. *Am. J. Physiol.* **1998**, *275*, F633–F650. [CrossRef]
52. Crambert, G.; Hasler, U.; Beggah, A.T.; Yu, C.; Modyanov, N.N.; Horisberger, J.-D.; Lelièvre, L.; Geering, K. Transport and pharmacological properties of nine different human Na,K-ATPase isozymes. *J. Biol. Chem.* **2000**, *275*, 1976–1986. [CrossRef]
53. Horisberger, J.D.; Kharoubi-Hess, S. Functional differences between α subunit isoforms of the rat Na,K-ATPase expressed in *Xenopus* oocytes. *J. Physiol.* **2002**, *539*, 669–680. [CrossRef]
54. Larsen, B.R.; Assentoft, M.; Cotrina, M.L.; Hua, S.Z.; Nedergaard, M.; Kaila, K.; Voipio, J.; MacAulay, N. Contributions of the $Na^+/K^+$-ATPase, NKCC1, and Kir4.1 to hippocampal $K^+$ clearance and volume responses. *Glia* **2014**, *62*, 608–622. [CrossRef]
55. Rosenthal, J.J.C.; Seeburg, P.H. A-to-I RNA editing: Effects on proteins key to neural excitability. *Neuron* **2012**, *74*, 432–439. [CrossRef]
56. Alon, S.; Garrett, S.C.; Levanon, E.Y.; Olson, S.; Graveley, B.R.; Rosenthal, J.J.C.; Eisenberg, E. The majority of transcripts in the squid nervous system are extensively recoded by A-to-I RNA editing. *eLife* **2015**, *4*, e05198. [CrossRef]

57. Vilallonga, G.D.; Almeida, A.C.G.; Ribeiro, K.T.; Campos, S.V.A.; Rodrigues, A.M. Hypothesized diprotomeric enzyme complex supported by stochastic modelling of palytoxin-induced Na/K pump channels. *R. Soc. Open Sci.* **2018**, *5*, 172155. [CrossRef]
58. McGrail, K.M.; Phillips, J.M.; Sweadner, K.J. Immunofluorescent localization of three Na,K-ATPase isozymes in the rat central nervous system: Both neurons and glia can express more than one Na,K-ATPase. *J. Neurosci.* **1991**, *11*, 381–391. [CrossRef]
59. Cameron, R.; Klein, L.; Shyjan, A.W.; Rakic, P.; Levenson, R. Neurons and astroglia express distinct subsets of Na,K-ATPase α and β subunits. *Mol. Brain Res.* **1994**, *21*, 333–343. [CrossRef]
60. Azarias, G.; Kruusmägi, M.; Connor, S.; Akkuratov, E.E.; Liu, X.L.; Lyons, D.; Brismar, H.; Broberger, C.; Aperia, A. A specific and essential role for Na,K-ATPase α3 in neurons co-expressing α1 and α3. *J. Biol. Chem.* **2013**, *288*, 2734–2743. [CrossRef]
61. Santos, D.O.C.; Rodrigues, A.M.; de Almeida, A.C.G.; Dickman, R. Firing patterns and synchronization in nonsynaptic epileptiform activity: The effect of gap junctions modulated by potassium accumulation. *Phys. Biol.* **2009**, *6*, 046019. [CrossRef]
62. Rodrigues, A.M.; Silva, D.B.; Miranda, M.F.; da Silva, S.C.B.; Santos, L.E.C.; Scorza, F.A.; Scorza, C.A.; Moret, M.A.; de Almeida, A.-C.G. The effect of low magnesium concentration on ictal discharges in a non-synaptic model. *Int. J. Neural Syst.* **2021**, *31*, 2050070. [CrossRef]
63. Teixeira, H.Z.; Almeida, A.C.G.; Infantosi, A.F.C.; Rodrigues, A.M.; Costa, N.L.; Duarte, M.A. Identifying essential conditions for refractoriness of Leão's spreading depression—Computational modeling. *Comput. Biol. Chem.* **2008**, *32*, 273–281. [CrossRef]
64. Rodrigues, A.M.; Ribeiro, K.T.; Melo, J.L.; Duarte, M.A.; Scorza, F.A.; Moret, M.A.; Pires, A.C.; Almeida, A.-C.G. Spreading depression spiral waves—Excitable media model. *Nonlinear Sci.* **2026**, *8*, 100151. [CrossRef]
65. Rodrigues, A.M.; Santos, L.E.C.; Covolan, L.; Hamani, C.; Almeida, A.C.G. PH during non-synaptic epileptiform activity—Computational simulations. *Phys. Biol.* **2015**, *12*, 056007. [CrossRef]
66. Ahmed, M.; Almeida, A.C.G.; Rodrigues, A.M.; Depannemaecker, D. Learning dynamics in biophysical spiking network models are shaped by KCC2/NKCC1 cotransporter stoichiometry. *Eur. J. Neurosci.* **2026**, *64*, e70596. [CrossRef]
67. Swift, F.; Tovsrud, N.; Enger, U.H.; Sjaastad, I.; Sejersted, O.M. The $Na^+/K^+$-ATPase α2-isoform regulates cardiac contractility in rat cardiomyocytes. *Cardiovasc. Res.* **2007**, *75*, 109–117. [CrossRef]


**Disclaimer/Publisher's Note:** The statements, opinions and data contained in all publications are solely those of the individual author(s) and contributor(s) and not of MDPI and/or the editor(s). MDPI and/or the editor(s) disclaim responsibility for any injury to people or property resulting from any ideas, methods, instructions or products referred to in the content.